Absolute density of the argon first excited states in plasmas used for carbon deposition as determined by absorption spectroscopy

ELSEVIER

Diamond and Related Materials 4 (1995) 1271–1276

DIAMOND AND RELATED MATERIALS

Absolute density of the argon first excited states in plasmas used for carbon deposition as determined by absorption spectroscopy

A.J.M. Buuron, D.K. Otorbaev, M.C.M. van de Sanden, D.C. Schram

Department of Physics, Eindhoven University of Technology, P.O. Box 513, 5600 MB Eindhoven, Netherlands

Received 17 February 1995; accepted in final form 19 June 1995

Abstract

In order to study the possible excitation transfer from argon metastables to the admixed species in an expanding cascaded arc plasma the densities of the Ar($3p^5 4s$) states in a deposition plasma were studied with absorption spectroscopy. For a purely argon plasma the Ar($3p^5 4s$) density lies in the range 10^{16}–10^{18} m^{-3} at a chamber pressure of 40 Pa. The effect on the densities of the addition of moderate amounts of methane and oxygen is small. The addition of hydrogen to the argon plasma leads to a rapid disappearance of the argon 4*s* states. Possible explanations are a lowering of the argon ion density by dissociative recombination and the direct excitation energy transfer with the H* ($n=2$, 3) levels.

Keywords: Cold plasma; Plasma diagnostics; Spectroscopy; Absorption

1. Introduction

The expanding thermal arc is capable of deposition layers of all types of carbon from amorphous hydrogenated carbon (a-C:H) to the crystalline forms graphite and diamond at high rates [1]. To this end, hydrocarbons and hydrogen and/or oxygen are admixed in the argon carrier gas. In Fig. 1 an outline of an expanding cascaded arc set up for carbon deposition is shown. The main feature of the method is the separation of the three functions: production, transport and deposition. The principal advantages of this method compared with conventional methods are high growth rates by the active particle transport towards the substrate, and flexibility in handling arc and substrate parameters. A cascaded arc plasma (4 mm diameter, 6 cm length), expanding in a vacuum chamber is used as a particle source. Specific features of this source are a high power dissipation (about 5 kW), a high plasma temperature of about 1 eV, and a long time of continuous operation (days). The carrier gas (argon) is injected at the beginning of the arc channel at a flow rate of about 100 standard cm^3 s^{-1}, which means a flow rate of 100 cm^3 s^{-1} normalized on a pressure of 10^5 Pa. The inlet pressure is of the order of 5×10^4 Pa. The ionization degree is typically about 10%, giving an electron density of the order of 10^{22} m^{-3}. As a consequence the arc plasma is close to partial local thermal equilibrium. A hydrocarbon (CH_4 or C_2H_2) can be injected (at rates of 0 to 10 standard cm^3 s^{-1}) at the end of the arc channel. Hydrogen can be admixed as an etching agent in the middle of the channel. By dissociation and charge exchange a beam of excited species, radicals and ions (Ar^{*+}, C^{*+}, H^{*+}, $C_xH_y^{*+}$) is created, expanding out of the end of the arc channel (the nozzle). The particles are accelerated to supersonic velocities of up to about 4000 m s^{-1}, pass through a shock and are transported further towards a substrate at subsonic velocities, decreasing down to a few hundreds of metres per second. A typical value for the chamber pressure is 10^2 Pa (for a-C:H deposition); in this case the shock can be observed at about 40 mm from the nozzle [2,3]. Beyond the

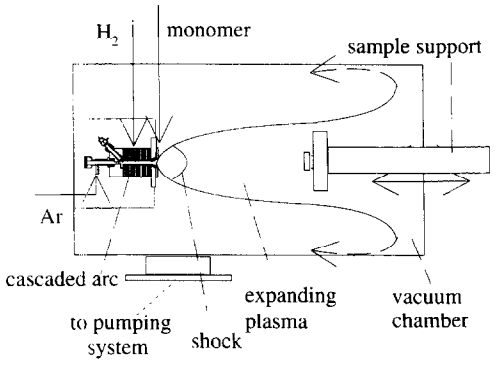

Fig. 1. The expanding cascaded arc set up for deposition.

SSDI 0925-9635(95)00303-7

shock, the total energy of the species decreases to about 0.5 eV. A typical value for the carbon ion flux is 10^{19} s^{-1}. The total transport time of all particles is relatively small (of the order of 10^{-4}–10^{-2} s), the radiative recombination is negligible; the loss of ionization by three particle recombination is less than 1% [2]. With this configuration, very high growth rates (200 nm s^{-1}) have been reached for amorphous carbon films at low substrate temperatures (20–100 °C) with argon–methane and argon–acetylene plasmas (ratio typically 100:1, flow rates in cubic centimetres per second). For higher deposition temperatures and with addition of H_2 to the gas flow, the growth rate is strongly reduced [4,5]. Diamond films have been deposited at 1000 °C in an argon–hydrogen–methane environment (ratio 20:20:0.2) at a rate of about 10 nm s^{-1}. The main factors determining the crystallinity of the film are the substrate temperature and the amount of hydrogen admixture in the argon flow.

The reactor parameters for crystalline diamond deposition are given in Table 1. An issue is the role of the Ar($3p^5 4s$) ($3p^5 4s$, $^3P_{0,1,2}$,$^1P_1$), two metastable and two resonant argon states (in the following referred to as argon 4s states), compared with that of the argon ion energy transfer processes to the admixed species. In Refs. [6,7] it was already demonstrated that, in an expanding argon plasma jet, the densities of the argon metastables are a factor of 10 lower than the ion density. In the present study the effect of the admixture of various gases used in deposition experiments, such as hydrogen, oxygen and methane, on the metastable densities was investigated in more detail.

Table 1
The reactor parameters for diamond deposition

Φ_{H_2}	3.2 cm^3 s^{-1}
Φ_{CH_4}	0.8 cm^3 s^{-1}
Φ_{O_2}	0.4 cm^3 s^{-1}
I_{arc}	45 A
Φ_{Ar}	58 cm^3 s^{-1}
$p_{chamber}$ (diamond deposition)	6×10^3 Pa
$p_{chamber}$ (spectroscopy)	40 Pa
d_{n-s}	127 mm

2. Experiment

To this end, the expanding plasma beam was monitored in axial and radial direction using the absorption spectroscopy technique described in Refs. [6,7]. In this method a cascaded arc is used as an external high intensity continuum light source [8]. In Fig. 2 the studied section of the argon system and the selected spectral transitions are shown. The four argon $3p^5 4s$ states under investigation can be distinguished in two metastable states ($^3P_0$ and $^3P_2$, also denoted by s_3 and s_5), and two resonant states ($^1P_1$ and $^3P_1$, s_2 and s_4). By means of the photodiode array, absorption measure-

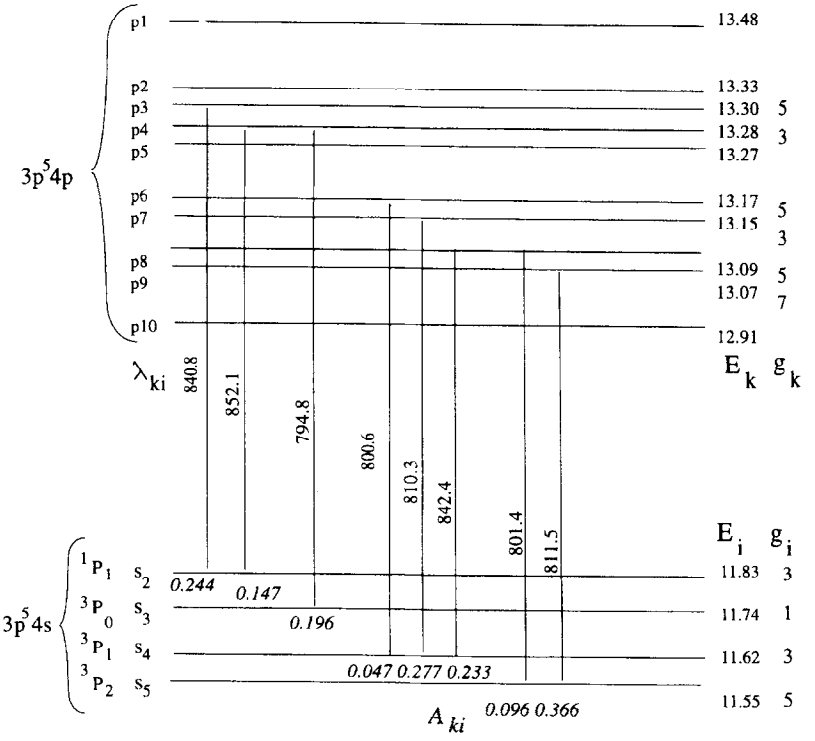

Fig. 2. The four argon $3p^5 4s$ states and the spectral transitions under investigation. Transition probabilities A_{ki}($\times 10^8$ s^{-1}), statistical weights g_i, g_k, wavelengths λ_{ki} (nm), and energies E_i, E_k (eV) [9] are indicated in the figure.

ments in the region 794–852 nm could be recorded simultaneously for the eight spectral transitions of argon coming from the four 4*s* sublevels and depicted in Fig. 2 [6,9].

At two interesting axial positions, close to the exit of the arc channel ($z = 27$ mm), and at the substrate location ($z = 127$ mm), 23 lateral measurements were carried out, 4 mm apart from each other. A specific Abel integration method was used to analyse the data, based on simulation of the density and of the temperature profiles and the spectral line shape in the expanding plasma jet [6]. The study was carried out on a plasma suited for amorphous carbon deposition at a chamber pressure of 40 Pa. For this special Abel inversion temperatures which are needed in the analysis have to be assumed. The temperatures were estimated based on experiences in emission spectroscopy and deposition experiments [1,10]. For the argon–methane plasma an axial temperature of 2500 K, for the argon–oxygen plasma a temperature of 3000 K, and for the argon–hydrogen plasma and the argon–hydrogen–methane–oxygen plasma an axial temperature of 2000 K were adopted. It should be noted that, for all the admixtures, no central dips were observed in the measured absorption data. The measured density profiles will be discussed in terms of a survey of reactions and rate coefficients in the expanding plasma.

3. Results and discussion

The main results are summarized in the following figures. In Figs. 3 and 4 the radial and axial profiles of the total density of the 4*s* states are given for the various gas admixtures. In order to discuss the result for each admixture separately in more detail, the axial decay of the densities for each of the four 4*s* sublevels is shown in the next figures. In Fig. 5(a) the axial decay of the argon 4*s* substrates, for two radial positions, on the axis and on the periphery of the plasma beam, in a pure argon plasma is recapitulated (from Ref. [6]). In Fig. 5(b) these densities are depicted normalized by statistical weights g_i (3, 1, 3, 5 respectively), and divided by the Boltzmann factor $\exp(-\Delta E/kT_e)$ (with ΔE with respect to the s_5 level), and using a value for the electron temperature T_e of 3000 K [10]. These normalized densities appear to be approximately equal (see Fig. 5(b)), indicating strong collisional coupling between the four states [11]. In Fig. 6 axial values of the densities of the four 4*s* substrates separately are depicted, for the various gas admixtures, again for the two radial positions are shown.

Comparing the profiles of the argon 4*s* states on the addition of the various admixtures to the argon carrier plasma with those for the purely argon plasma, the following features can be observed.

(1) The shape and the values of the radial profiles are only slightly affected by the admixture of oxygen and methane in the nozzle. The admixture of hydrogen (in the arc), both separately and in the combination of the three gases used for diamond deposition, leads to narrower profiles and substantially lower density values.

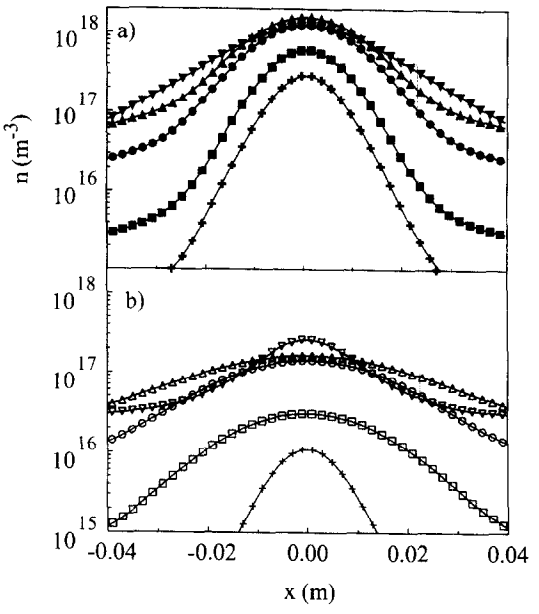

Fig. 3. Radial profiles of the total density of the argon 4*s* state on the addition of various gases: ▲, △, standard argon plasma; ●, ○, 0.8 cm^3 CH_4 s^{-1} in the nozzle; ▼, ▽, 0.4 cm^3 O_2 s^{-1} in the nozzle; ■, □, 3.2 cm^3 H_2 s^{-1} in the arc; +, ✚, combination of the three admixtures (diamond condition); (a) $z = 27$ mm; (b) $z = 127$ mm.

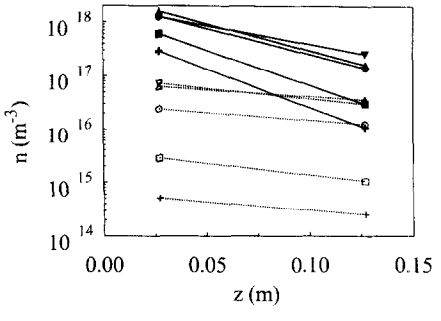

Fig. 4. Axial values of the total density of the argon 4*s* state on the addition of various gases. The symbols are the same as in Fig. 3. Radial positions are as follows: ▼, ▲, ●, ■, ✚, $x = 0$ mm; ▽, △, ○, □, +, $x = 40$ mm. Note that here the lines merely serve to connect the associated data points and do not reflect an actually measured dependence.

(2) In a purely argon plasma, Fig. 5(b), the substrates appear to be thermally populated by the rapid interstate mixing by electronic collisions [11]. The densities per statistical weight and corrected for the Boltzmann exponent are approximately equal for most of the positions. On addition of the various gases it is possible to show from the data, presented in Fig. 6, that this equilibrium is perturbed. Particularly for the off-axis positions (the open symbols) the electronic coupling appears to be bad. This may be due to a lower electron density caused by the admixture. In particular, the methane admixture in the nozzle seems to have a perturbing effect at the

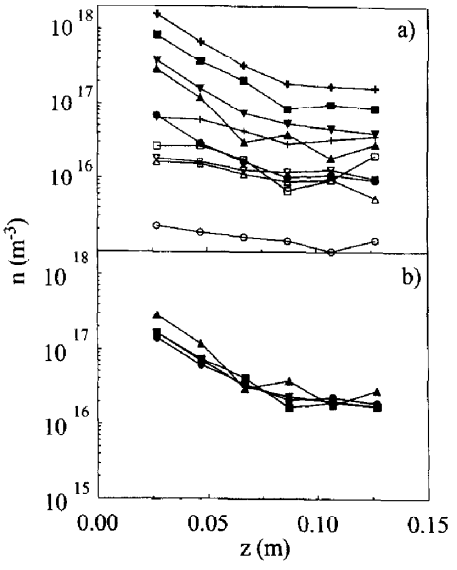

Fig. 5. Axial decay of the densities of the argon 4s substrates, in a purely argon plasma: ▲, △, S_2; ●, ○, s_3; ▼, ▽, s_4; ■, □, s_5; ✚, +, total 4s density. Radial positions are as follows: ▲, ●, ▼, ■, ✚, $x=0$ mm; △, ○, ▽, □, +, $x=40$ mm.

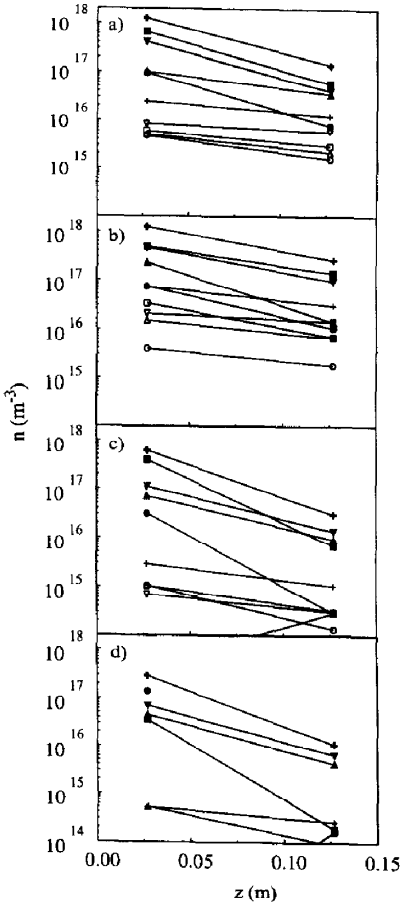

Fig. 6. Axial decay of the densities of the argon 4s substrates on the addition of various gases: (a) 0.8 cm^3 CH_4 s^{-1} in the nozzle; (b) 0.4 cm^3 O_2 s^{-1} in the nozzle; (c) 3.2 cm^3 H_2 s^{-1} in the middle of the arc; (d) combination of the gas admixtures of (a)–(c). The symbols are the same as in Fig. 5.

plasma edge, probably owing to a bad mixing into the plasma core. Also, the inaccuracy in the determination of 4s densities on the off-axis positions may be too large, although the total densities (the + symbols) yield a realistic picture.

Concerning the positions at the plasma axis (the solid symbols), we note the following. For the cases of methane and oxygen addition, Figs. 6(a) and 6(b), the coupling is still reasonable for the metastable states. The densities for the radiative levels (triangles) are no longer equal. The reason for this is not clear. For the cases of hydrogen and the combined addition, Figs. 6(c) and 6(d), it is just reversed. The densities of the resonant states remain approximately equal, while those of the metastable states have decreased strongly at the position $z=127$ mm. The populating of these states to the resonant states has to be provided by electronic and heavy particle collisional coupling to the resonant states, which appears to be inadequate.

The relative effect of the argon metastables in exchange processes compared with that of the ions can be estimated by considering the rate coefficients for the various reactions. A problem is that in the literature often values for cross-sections and rate coefficients are given which are only valid in the given specific conditions (e.g. room temperature). Therefore, the rate constants for the temperatures in our case have often been obtained by extrapolation of literature values, starting from the relationship $K=\langle\sigma(v)v\rangle$ (integration over the velocity distribution). To this end, two assumptions were made. Unless stated otherwise, the cross-section is taken to be independent of v, so that K can be expressed as $\sigma\bar{v}$, and for $\bar{v}$ the mean Boltzmann speed is taken, which is proportional to $T^{1/2}$ [12,13]. We have of course proof that the velocity distribution is maxwellian.

(3) For the present small amounts of methane and oxygen admixture, Figs. 3, 4, 6(a) and 6(b), both the ionization degree of the plasma and the argon 4s densities are hardly affected compared with that of a pure argon plasma. The electron densities remain of the order of 10^{19} m^{-3}. This has been established by emission spectroscopy [10], and probe measurements [14] respectively. These findings support the assumption that the argon 4s densities are coupled to the ion density. The ion densities are a factor of 10 higher than the argon 4s densities. On admixture of methane in a pure argon plasma the following reactions are of importance:

$$Ar^+ + CH_y \xrightarrow{K_1} Ar + CH_x^+ + (y-x)H \quad (1)$$

$$Ar^m + CH_y \xrightarrow{K_2} Ar + CH_y^+ + e^- \quad (2)$$

$$Ar^m + CH_y \xrightarrow{K_3} Ar + CH_x + (y-x)H \quad (3)$$

$$e^- + CH_y^+ \xrightarrow{K_4} CH_x + (y-x)H \quad (4)$$

For $y=4$ (starting with methane) the rate coefficients at 2500 K can be estimated (using values available in the cited literature): $K_1=3.4\times10^{-15}$ m^3 s^{-1} [15], $K_1(x=4)=4.3\times10^{-16}$ m^3 s^{-1} [16,17], $K_1(x=3)=2.1\times10^{-15}$ m^3 s^{-1} [16,17], $K_3=(0.9-1.7\times10^{-15}$ m^3 s^{-1} [13,18], $K_4\approx10^{-13}$ m^3 s^{-1} [19,20].

Direct dissociation or ionization of CH_4 by electronic collisions at the low T_e values is negligible because the thresholds for these processes are about 10 eV and 13 eV respectively [21]. The cross-section for reaction (4) is orders of magnitude larger than that for reaction (3) and so the dissociative recombination reaction is the predominant dissociation mechanism. For K_2 no data are available. Penning ionization of CH_4 can most probably be ruled out because of its ionization potential of 12.6 eV, which is 0.9 eV higher than the highest metastable state. The ionization potentials of the CH_x radicals, however, are 11.1 eV, 10.4 eV and 9.8 eV for $x=1,2,3$ respectively [22], so Penning ionization of these species can easily occur. No rate coefficients are available but an indication for their values may be obtained from the comparable reaction on acetylene (ionization potential, 11.4 eV), i.e.

$$Ar^m + C_2H_2 \xrightarrow{K_2'} Ar + C_2H_2^+ + e^- \quad (5)$$

for which the rate coefficient is known: $K_2'=1.61\times10^{-15}$ m^3 s^{-1} [15]. Now, comparing the products of rate constants and densities, we may conclude that the role of the metastables is limited and that the most important mechanism for the creation of active (hydro)-carbon species is the direct charge exchange with the argon ions followed by dissociative recombination.

(4) On the admixture of hydrogen, and the combination of the three gases methane, oxygen and hydrogen, the following features can be observed.

- On both axial positions the argon 4*s* densities are much lower than those for the pure argon plasma.
- The density profiles are narrower in comparison with pure argon case.

The following reactions are proposed to account for the loss of argon 4*s* states.

- Assuming that all 4*s* states come from recombination of argon ions, the loss of argon ions by charge transfer followed by dissociative recombination is responsible for the decrease in production of the 4*s* densities:

$$Ar^+ + H_2 \xrightarrow{K_6} H_2^+ + Ar \quad (6)$$

$$Ar^+ + H_2 \xrightarrow{K_7} ArH^+ + H \quad (7)$$

$$e^- + ArH^+ \xrightarrow{K_8} Ar + H^* \quad (8)$$

$$e^- + H_2^+ \xrightarrow{K_9} H + H^* \quad (9)$$

Reactions (8) and (9) are very effective with rate constants K_8 and K_9 of the order of $10^{-14}-10^{-13}$ m^3 s^{-1}. In Ref. [23] an approximately constant cross-section of the order of 10 Å^2 is given for reaction (6). For K_7 the temperature dependence is even given. For K_7 estimates are also given in Ref. [24]; $K_6=0.55\times10^{-15}$ m^3 s^{-1} [23], $K_7=1.13\times10^{-15}$ m^3 s^{-1} [23], $K_7=1.39\times10^{-15}$ m^3 s^{-1} [24]. In this view the observed decrease in metastables in the plasma is consistent with the observed decrease in the ion density in argon–hydrogen plasmas [25,26].

- Direct interaction (excitation transfer) with the H* ($n=2,3$) levels [27,28] may also be responsible:

$$Ar^m + H \xrightarrow{K_{10}} Ar + H^*(n=2) + 1.3\ eV \quad (10)$$

with $K_{10}=0.62\times10^{-15}$ m^3 s^{-1} for a temperature of 2000 K [27].

The typical narrow profiles could be caused by the following mechanisms.

- Again the predominant mechanism may be that the admixture of hydrogen leads to a substantial loss of ions and thus to a lower 4*s* density in the core. As a result, the resonance radiation has decreased considerably, which leads consequently to a lower production of 4*s* states in the periphery by radiation capture.
- The mixing of the injected hydrogen into the argon plasma core may be bad, leading to a relatively high reduction of the 4*s* density in the periphery (again by loss of ionization). Also, it could be an indication for the recirculation of H_2 [7], which will be more abundant than atomic hydrogen in the edges of the plasma core. In this case for example the following loss channel is present:

$$H_2 + Ar^m \xrightarrow{K_{11}} ArH^* + H \quad (11)$$

with $K_{11}=0.17\times10^{-15}$ m^3 s^{-1} [13] or $K_{11}=0.28\times10^{-15}$ m^3 s^{-1} [18].

4. Conclusion

We conclude the following. Addition of hydrogen affects the metastable density drastically. Most likely this is due to two reasons: (a) the hydrogen-induced loss of ionization; (b) the excitation transfer between argon and hydrogen atoms. In the expansion itself the decrease in the argon 4*s* densities is stronger than in the expansion of a purely argon plasma, so further interaction takes place between the hydrogen and the argon 4*s*. No interaction of the metastables with methane was observed, confirming the negligible role of the argon metastables in the dissociation of CH_4. Addition of small

amounts of oxygen has no effect on either the ion density or the 4s densities.

Acknowledgements

This work was made possible by the financial support of Electricité de France, as a consequence of a collaboration with the Eindhoven University of Technology (Contract M60L04/7B006/EL447). D.K. Otorbaev acknowledges support from the Eindhoven University of Technology. The work of M.C.M. van de Sanden has been made possible by the Royal Netherlands Academy of Arts and Sciences. Furthermore, the work of J.J. Beulens, M. Schuwer, H. de Jong, T. Kiers, M.J.F. van de Sande and B. Hüsken in developing and building the spectroscopy set-up, including the home-made photodiode array device, is gratefully acknowledged.

References

[1] A.J.M. Buuron, J.J. Beulens, P. Groot, J. Bakker and D.C. Schram, *Thin Solid Films, 212* (1991) 282.
[2] M.C.M. van de Sanden, J.M. de Regt and D.C. Schram, *Phys. Rev. E, 47* (1993) 2792.
[3] M.C.M. van de Sanden, J.M. de Regt and D.C. Schram, *Plasma Sources Sci. Technol, 3* (1994) 501. M.C.M. van de Sanden, R. van den Bercken and D.C. Schram, *Plasma Sources Sci. Technol., 3* (1994) 511.
[4] H. Kersten and G.M.W. Kroesen, *J. Vac. Sci. Technol. A, 8* (1990) 38.
[5] P.K. Bachmann, H. Lydtin, D.U. Wiechert, J.J. Beulens, G.M.W. Kroesen and D.C. Schram, in T.S. Sudarshan and D.G. Bhat (eds.), *Proc. 3rd Int. Conf. on Surface Modification, Surface Modification Technologies III*, The Minerals, Metals and Materials Society, Warrendale, PA, 1990.
[6] A.J.M. Buuron, D.K. Otorbaev, M.C.M. van de Sanden and D.C. Schram, *Phys. Rev. E, 50* (1994) 1383.
[7] D.K. Otorbaev, A.J.M. Buuron, M.C.M. van de Sanden and D.C. Schram, *J. Appl. Phys., 76* (1994) 4499.
[8] A.T.M. Wilbers, G.M.W. Kroesen, C.J. Timmermans and D.C. Schram, *Meas. Sci. Technol., 1* (1990) 1326.
[9] W.L. Wiese, M.W. Smith and B.M. Miles, *Atomic Transition Probabilities, NSRDS-NBS 22*, Washington, DC, 1969.
[10] J.J. Beulens, *Ph.D. Thesis*, Eindhoven University of Technology, Eindhoven, 1993.
[11] J.-L. Delcroix, C.M. Ferreira and A. Ricard, in G. Bekefi (ed.), *Principles of Laser Plasmas*, Wiley, New York, 1976.
[12] M.H. Gordon and C.H. Kruger, *Phys. Fluids B, 5* (1993) 1014.
[13] L.G. Piper, J.E. Velazco and D.W. Setser, *J. Chem. Phys., 59* (1973) 3323.
[14] Z. Qing, M.C.M. van de Sanden, M.J. de Graaf, D.K. Otorbaev, G.J. Meeusen, A.J.M. Buuron and D.C. Schram, in J. Harry (ed.), *Proc. 11th Int. Symp. on Plasma Chemistry, Loughborough, 1993*, Vol. 4, p. 1374.
[15] M.T. Bowers and J.B. Laudenslager, in G. Bekefi (ed.), *Principles of Laser Plasmas*, Wiley, New York, 1976.
[16] A. Inspektor, U. Carmi, R. Avni and H. Nickel, *Plasma Chem. Plasma Process., 1* (1981) 377.
[17] C.E. Melton, *J. Chem. Phys, 33* (1960) 647.
[18] M. Bourène and J. Le Calvé, *J. Chem. Phys., 58* (1973) 1452.
[19] K. Tachibana, M. Nishida, H. Harima and Y. Urano, *J. Phys. D, 17* (1984) 1727.
[20] J.N. Bardsley and M.A. Biondi, in D. Bates and B. Bederson (eds.), *Advances in Atomic and Molecular Physics*, Vol. 6, Academic Press, New York, 1970.
[21] H. Winters, *J. Chem. Phys., 63* (1975) 3462.
[22] D.R. Lide (ed.), *Handbook of Chemistry and Physics*, CRC Press, Boca Raton, FL, 1991.
[23] A.V. Phelps, *J. Phys. Chem. Ref. Data, 21* (1992) 883.
[24] A.B. Rakshit and P. Warneck, *J. Chem. Phys., 73* (1980) 2673.
[25] M.J. de Graaf, R. Severens, R.P. Dahiya, M.C.M. van de Sanden and D.C. Schram, *Phys. Rev. E, 48* (1993) 2098.
[26] R.F.G. Meulenbroeks, A.J. van Beck, A.J.G. van Helvoort, M.C.M. van de Sanden and D.C. Schram, *Phys. Rev. E, 49* (1994) 4397.
[27] M.A.A. Clyne, M.C. Heaven, K.D. Bayes and P.B. Monkhouse, *Chem. Phys., 47* (1980) 179.
[28] R.L. Vance and G.A. Gallup, *J. Chem. Phys., 72* (1980) 894.